GEOLOGICAL SURVEY OF CANADA
OPEN FILE 7549

Results from a Magnetotelluric and Rock Property Study near Churchill, Manitoba

B. Bancroft, J.A. Craven, R.J. Enkin, M.P.B. Nicolas, B. Roberts

2014

Natural Resources Canada
Ressources naturelles Canada

Canada

GEOLOGICAL SURVEY OF CANADA
OPEN FILE 7549

Results from a Magnetotelluric and Rock Property Study near Churchill, Manitoba

B. Bancroft[1], J.A. Craven[2], R.J. Enkin[3], M.P.B. Nicolas[4], B. Roberts[2]

[1] 47 Kalbrook Street, Ottawa Ontario K2T 1A6
[2] Geological Survey of Canada, 615 Booth Street, Ottawa, Ontario, K1A 0E9
[3] Geological Survey of Canada, 9860 West Saanich Road, Sidney, British Columbia V8L 4B2
[4] Manitoba Geological Survey, 360-1395 Ellice Avenue, Winnipeg, Manitoba R2G 3P2

2014

doi:10.4095/293454

This publication is available for free download through GEOSCAN (http://geoscan.ess.nrcan.gc.ca/).

Recommended citation
Bancroft, B., Craven, J.A., Enkin, R.J., Nicolas, M.P.B., and Roberts, B., 2014. Results from a Magnetotelluric and Rock Property Study near Churchill, Manitoba; Geological Survey of Canada, Open File 7549, 21 p. doi:10.4095/293454

Contents

Figures 3

Introduction 4

Lithostratigraphic Framework 4

The Magnetotelluric (MT) Method 6

MT Data Processing and Modeling 9

Rock Core Sample Processing and Measurement 10

Conclusions 14

Acknowledgements 14

References 15

Appendix 1. AAV Models, comparison i

Appendix 2. Averaged Data and Fit Curves from the 1-D Inversion ii

Appendix 3: Sample Rock Property Data iii

Figures

Figure 1: Lithostratigraphic framework of the Paleozoic in the Hudson Platform. Modified from Zhang (2010). 5
Figure 2: Map of the study area. The dashed line is the location of the section shown in Figure 7. Modified from Roberts and Craven (2012). 6
Figure 3: Apparent resistivity and phase data for site Chu_36. Sections of low-quality data (greyed) were omitted from the 1-D inversions due to its poor quality or obvious departures from 1-D behavior. 8
Figure 4: Example of the arithmetic average inversions conducted in this study at site Chu_36. The models resulting from inversion of the XY and YX data are shown alongside the inversion of the arithmetic average. The response of the arithmetic model is superimposed on the average apparent resistivity and phase data plotted as symbols. 9
Figure 5: Resistivity and skeletal density of rock samples detailed in Appendix 1 categorized by stratigraphic unit. Trends in the data are highlighted in grey. The points are coloured by susceptibility, blue: ~3x10-6 SI, green: ~2x10-5 SI, yellow: ~5x10-5, red: ~3x10-4 SI. 11
Figure 6: Inversion results at Chu_36 plotted alongside the rock property derived resistivities. 12
Figure 7: Schematic cross-section of geological strata for the eight sites of this study based on the inversion of the MT data and rock property data. 13
Figure 8: 1-D Inversion results from arithmetic averages of data. Pseudo-scale bar shows relative separation between sites along the dashed line in Figure 1. i
Figure 9: Averaged apparent resistivity and phase diagrams with the fit curved obtained from the inversion. Data in grey were not used in the inversion. ii
Figure 10: Petrophysical Data Plots. iv

Introduction

In 2012, a magnetotelluric (MT) survey was conducted by Roberts and Craven (2012) across the Upper Ordovician section of the Paleozoic strata near Churchill, Manitoba, at the margin of the Hudson Bay Basin. This survey sought to evaluate MT as method to identify potential source or reservoir rocks in a region whose resource potential is currently being re-evaluated (Lavoie et al., 2013). Due to the fact the Upper Ordovician section of the Paleozoic strata in this region is close to the surface and potentially contains both reservoir rocks (e.g. porous hydrothermally altered limestone) and source rocks (e.g. oil shales within the Red Head Formation) a better understanding of this region could assist informed exploration at deeper portions of the Hudson Bay Basin. This study focuses on eight of the 55 MT sites that were located close to the Churchill airport and the town of Churchill itself. The data from these sites were not analyzed by Roberts and Craven (2012) due to the considerable electromagnetic (EM) noise present in the data. The MT sites used in the current analysis are close to a stratigraphic well. Electrical rock property asassessments have been made on the core from this well and are also reported herein. Results from the inversion of the data near Churchill are compared to the rock property information to determine if a reasonable estimation of the stratigraphic column can be made from the MT data.

Lithostratigraphic Framework

The Hudson Platform is comprised of the Hudson Bay Basin and smaller adjoining Foxe and Moose River basins deposited upon Precambrian Churchill and Superior provinces. Although it has a surface area larger than the major oil and gas producing intratronic basins of central North America, the Platform is the least well studied. The Paleozoic stratigraphy (Figure 1) within the Platform is summarized by Sanford, Norris and Bostock (1968), Norris (1993), Hamblin (2008) and Zhang (2008). In the Hudson Bay Lowland, primarily marine deposition occurred periodically from the Late Ordovician to Late Devonian. Composed of carbonates with small amounts of evaporite and shale, the Upper Ordovician portion of the succession is divided into the Bad Cache Rapids and Churchill River groups with the Red Head Rapids Formation lying unconformably on top of basement (Nelson, 1963, 1964). The Bad Cache Rapids Group is composed of a dark grey or brownish grey limestone overlying a thin sequence of clastic rocks, and is rich in corals, gastropods, nautiloid cephalopods, algae, crinoids and trace fossils.

The thickness of the Bad Cache Group thickens only 5 m from Hudson Bay Lowland (~ 76.7 m) to offshore (Zhang and Trends in the data are highlighted in grey Barnes, 2007). The Churchill River Group, about 103–105 m thick in the Hudson Bay Lowland and offshore areas (Zhang and Barnes, 2007), is a greenish grey or greyish brown argillaceous limestone relatively devoid of macrofossils. Sanford (in Heywood and Sanford, 1976) inserted the "Boas River shale" between the Bad Cache Rapids and Churchill River groups without seeing the contact in outcrop. Zhang (2008) demonstrates the regional nature of this shale by finding correlative units on Southampton Island. The third primary unit in the area is Red Head Rapids Formation named by Nelson (1963). Exposed along the Churchill River in Manitoba, this unit is composed of 14 m of relatively unfossiliferous microcrystalline dolomite. The Red Head Rapids Formation exhibits a distinctive orange-tan colour, in contrast to the grey of the Bad Cache Rapids and Churchill River groups. Zhang (2008) documents two new findings within the Red Head Rapids Formation on Southampton Island. First, there exist three oil shale intervals within the laminated limestone and, secondly, a carbonate breccia unit is located between laminated limestone and certain biostromal units. Lavoie et al. (2011) document in the subsurface of the Platform the presence of hydrothermally altered dolomites, which is a relatively new style of play in the Williston Basin.

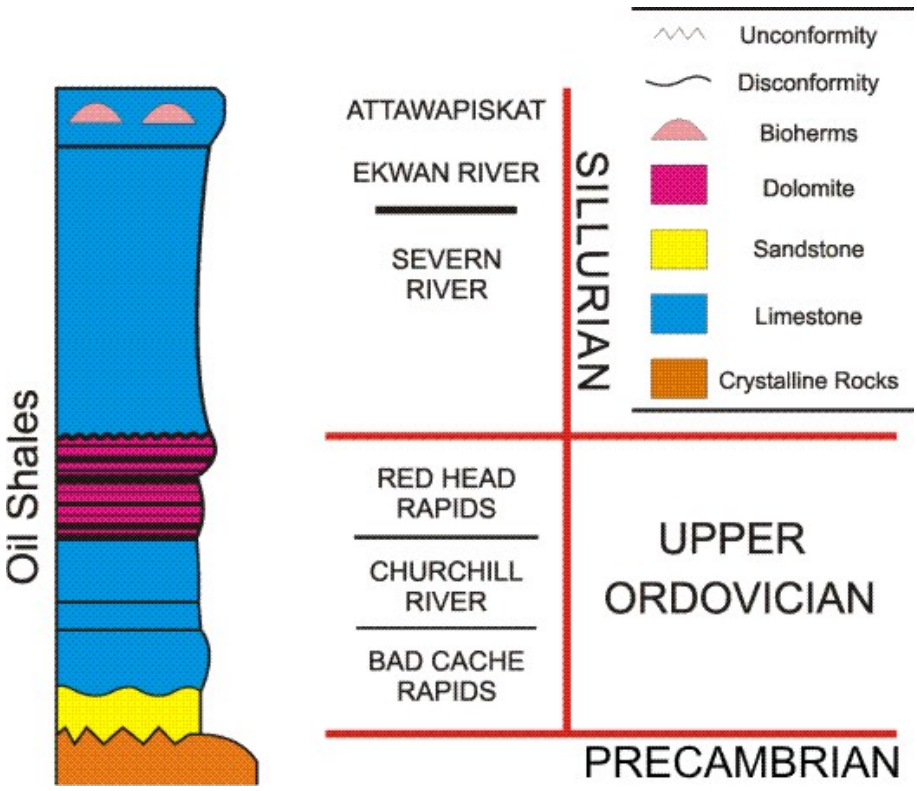

Figure 1: Lithostratigraphic framework of the Paleozoic in the Hudson Platform. Modified from Zhang (2010).

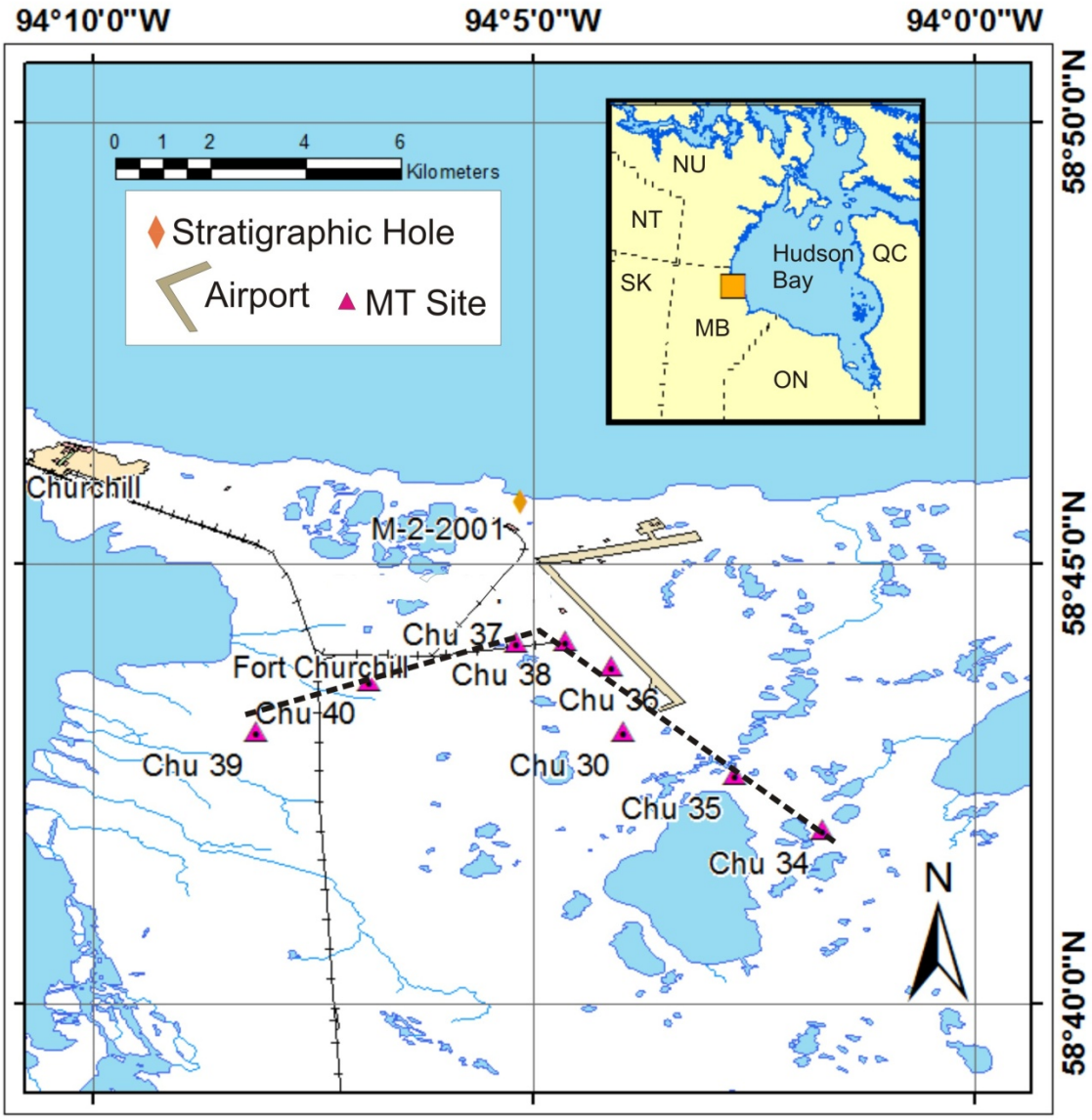

Figure 2: Map of the study area. The dashed line is the location of the section shown in Figure 7. Modified from Roberts and Craven (2012).

The Magnetotelluric (MT) Method

The MT method uses measurements of naturally-occurring, transient electric and magnetic fields at the surface to produce an estimate of subsurface electrical conductivity (Chave and Jones, 2012). The signals are transformed into the frequency domain and used to calculate a complex impedance between the two measurements which can equivalently be expressed in terms of apparent resistivity ($\boldsymbol{\rho}_a$)and phase ($\boldsymbol{\Phi}$) in terms of frequency. If $E_i(\omega)$and $H_j(\omega)$ are horizontal electric and magnetic field components for a given frequency (ω), then the impedance $\boldsymbol{Z}(\omega)$ is defined as :

$$Z_{ij}(\omega) = \frac{E_i(\omega)}{H_j(\omega)} \qquad \text{where i} = \text{x, y;} \quad \text{j} = \text{x, y}$$

A separate apparent resistivity can be calculated from each of the four impedances as:

$$\boldsymbol{\rho}_a = \frac{1}{\omega\mu_0}|\mathbf{Z}|^2$$

where μ_0 is the permeability of free space. Electromagnetic signals travel through conductive material diffusively, and the depth of penetration increases with the period (i.e. the inverse of frequency) of the signal. The skin depth is defined as the distance over which a diffusive EM signal is attenuated to 1/e of its original amplitude. The apparent resistivity can be considered as the average resistivity from the surface to a depth equal to the skin depth. Thus using the fact that lower frequencies penetrate deeper in the Earth, the depth variation of resistivity can be defined. The phase ($\boldsymbol{\Phi}$) of the tensor elements

$$\boldsymbol{\Phi} = tan^{-1}(\boldsymbol{Z})$$

is useful because it is sensitive to changes in resistivity with depth.

The apparent resistivity and phase are transformed into estimates of true subsurface resistivity using inversion algorithms based on approximations of the earth as either spatially variant only with depth (i.e. 1-D) or variant in two or three directions (i.e. 2-D or 3-D models). The decision to use a 1-, 2- or 3-D inversion algorithm is based on the known complexity of the geology in the region and the manifestation of that complexity in the MT data (apparent resistivities and phases). Important for our study is the 1-D case, wherein two of the four impedance elements are equal but reverse polarization, (i.e. Z_{xy} equal to -Z_{yx}) whereas the remaining two elements of the impedance tensor are zero. These relationships can also be exhibited through similar corresponding apparent resistivities and phases offset by 180 degrees.

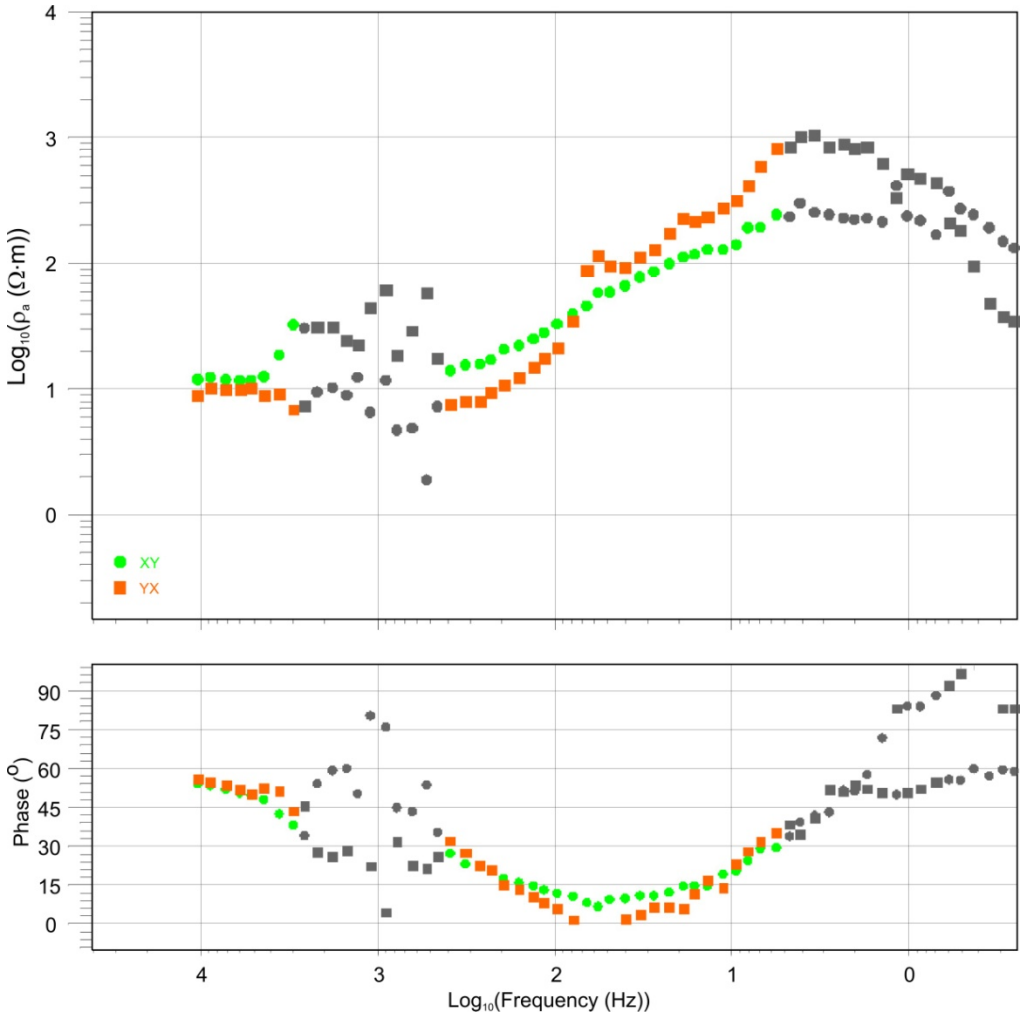

Figure 3: Apparent resistivity and phase data for site Chu_36. Sections of low-quality data (greyed) were omitted from the 1-D inversions due to its poor quality or obvious departures from 1-D behavior.

Typically, shales are the most conductive sedimentary lithology (approx. 10 Ω ·m) due to the electrical conductivity along clay surfaces. In water-saturated condition, limestones are typically resistive (> 100 Ω ·m), and sandstones typically have resistivities of the order 100 Ω ·m. While the subsurface resistivity provides an indication of the lithological unit, it can also be sensitive to electrically conductive material such as graphite or interconnected grains of metallic sulphides. Saline fluids, such as basinal brines, decrease resistivity through ionic conduction within the pore space. The sensitivity of MT to these geological constituents means the method can provide unique geological information that is complementary to other geophysical methods.

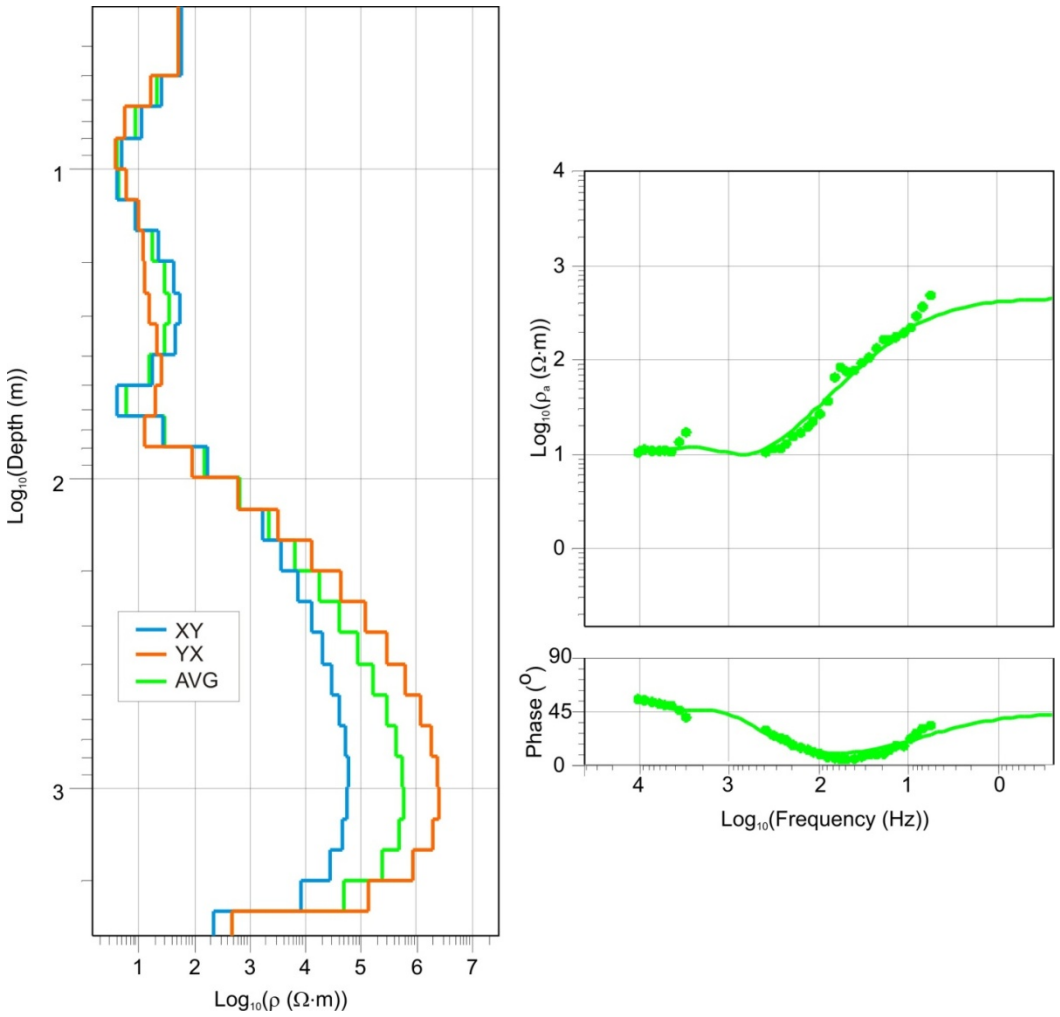

Figure 4: Example of the arithmetic average inversions conducted in this study at site Chu_36. The models resulting from inversion of the XY and YX data are shown alongside the inversion of the arithmetic average. The response of the arithmetic model is superimposed on the average apparent resistivity and phase data plotted as symbols.

MT Data Processing and Modeling

The complete dataset described by Roberts and Craven (2012) was imported into the Geotools MT package. The data for the eight sites (Figure 2) not analyzed by Roberts and Craven (2012) were then modeled using the 1-D Occam inversion technique (Constable et al., 1987). An Occam inversion produces a conservative estimate of the subsurface structure required to generate a synthetic response that matches the data at each site. Frequency bands considered to be overly influenced by EM interference associated with human infrastructure were removed prior to inversion. The noise sources are discussed in more detail in Roberts and Craven (2012). Data were also eliminated where there was evidence of a clear departure from the 1-D behavior of the resistivities and phases as described above. An example of data eliminated is shown in Figure 3.

Two inversions for each site utilizing the edited xy and yx apparent resistivities and phases were computed to determine the key bands exhibiting 1-D behavior. Next, an arithmetic average (see Figure 4) of the two 1-D responses was computed and inverted to create a single model for each site. This process was repeated for all sites in the study and final models are shown in Appendix 1 and responses in Appendix 2. The inversion process gave reasonable results comparable to those observed earlier by Roberts and Craven (2012).

Rock Core Sample Processing and Measurement

Following the procedures outlined by Enkin et al. (2012), rock property measurements begin with drying each core sample for 24 hours at 40^{o}C, followed by measurement of the dry mass before vacuum-impregnation with deionized, distilled water for 24 hours. Impedances are measured using a spectrum analyzer at five frequencies per decade from 1 MHz to 0.03 Hz. The real resistance is measured as the zero-frequency extrapolation of the complex impedance frequency curve. The sample resistivity is determined after multiplication by the cross sectional area and division by the length of the sample. All but one core sample used for this study were taken from the M-2-2001 stratigraphic well (Figure 1). The one exception is based on hand samples of the local Precambrian units. The samples and measurement results, including density, porosity, magnetic susceptibility, electrical resistivity and chargeability are detailed in Appendix 3 and plotted according to stratigraphic unit in Figure 5.

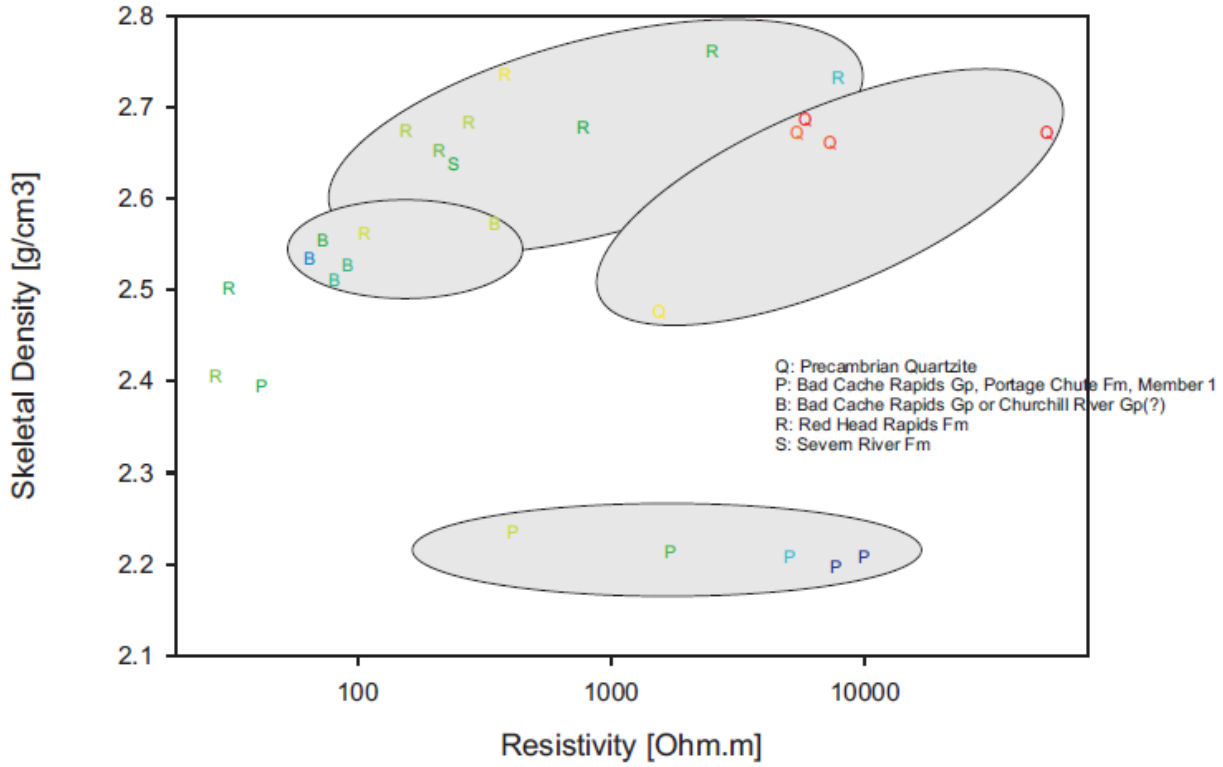

Figure 5: Resistivity and skeletal density of rock samples detailed in Appendix 1 categorized by stratigraphic unit. Trends in the data are highlighted in grey. The points are coloured by susceptibility, blue: ~3x10-6 SI, green: ~2x10-5 SI, yellow: ~5x10-5, red: ~3x10-4 SI.

The Precambrian samples (Figure 5 and Figure 10) display typical properties of crystalline rocks. The Portage Chute sandstones are high porosity, low density, and relatively high resistivity. The one coarse sandstone (sample 6), has low resistivity, but in general the resistivities tend to overlap with those of the Precambrian units. The Bad Cache/Churchill River samples are the most conductive of the samples, but overlap with the argillaceous units of the Red Head Rapids Group. In general, the Red Head Rapids Group can be differentiated from a rock property perspective in terms of the clay content. The argillaceous samples are generally higher density, lower porosity, higher resistivity, and higher chargeability. These properties can be explained with increased clay content filling pores.

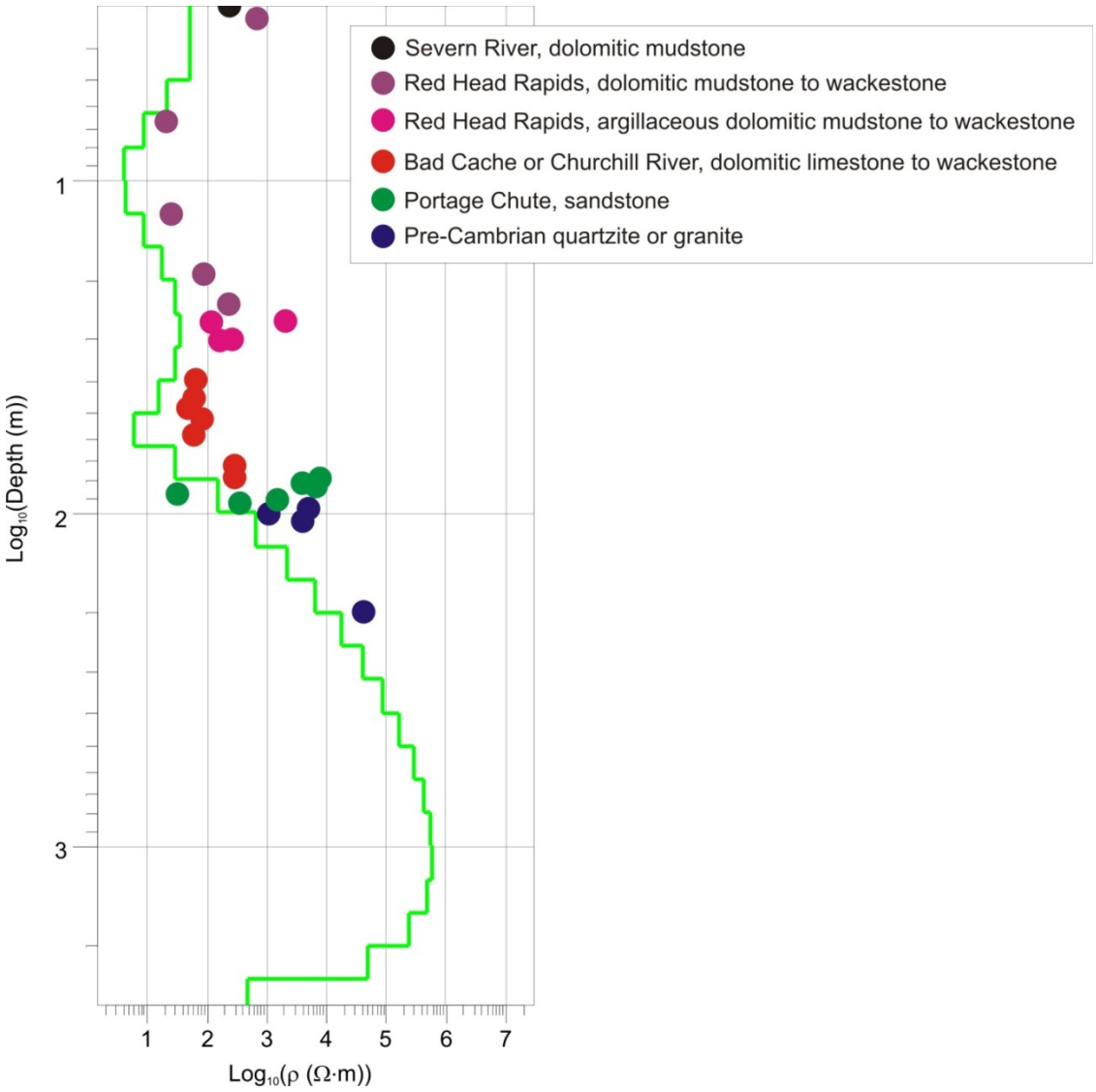

Figure 6: Inversion results at Chu_36 plotted alongside the rock property derived resistivities.

The match of the inversion results at site Chu_36 with the rock property data is shown in Figure 6. In general there is good agreement in the trends of the two datasets, but the inverted results are approximately an order of magnitude more conductive than the rock property data. Some of the differences between the rock property and inversion results can be explained by the nature of the physics involved in MT. Electrical currents are not induced as strongly in resistive units and so MT inversion cannot resolve these units and will tend to underestimate the true resistivity. Due to these differences, our method to analyze the inversions matched the resistivity values obtained from each inversion to the nearest resistivity values from the core samples. When this process resulted in a unit inconsistent with the

expected stratigraphic order, the unit was replaced with the unit with the closest resistivity value consistent with the stratigraphic column in Figure 1.

A cartoon section (Figure 7) was constructed utilizing the script on all eight models. The pseudo cross-section demonstrates a predominantly layered appearance validating the 1-D methodology utilized. The thicknesses observed in Figure 7 are reasonable as well. It is important to note that thickness of the units was not used as a constraint in the modeling. Indeed, no a priori information was used for the inversion. MT data can identify layer interfaces given appropriate resistivity contrasts and sufficiently precise data measurement.

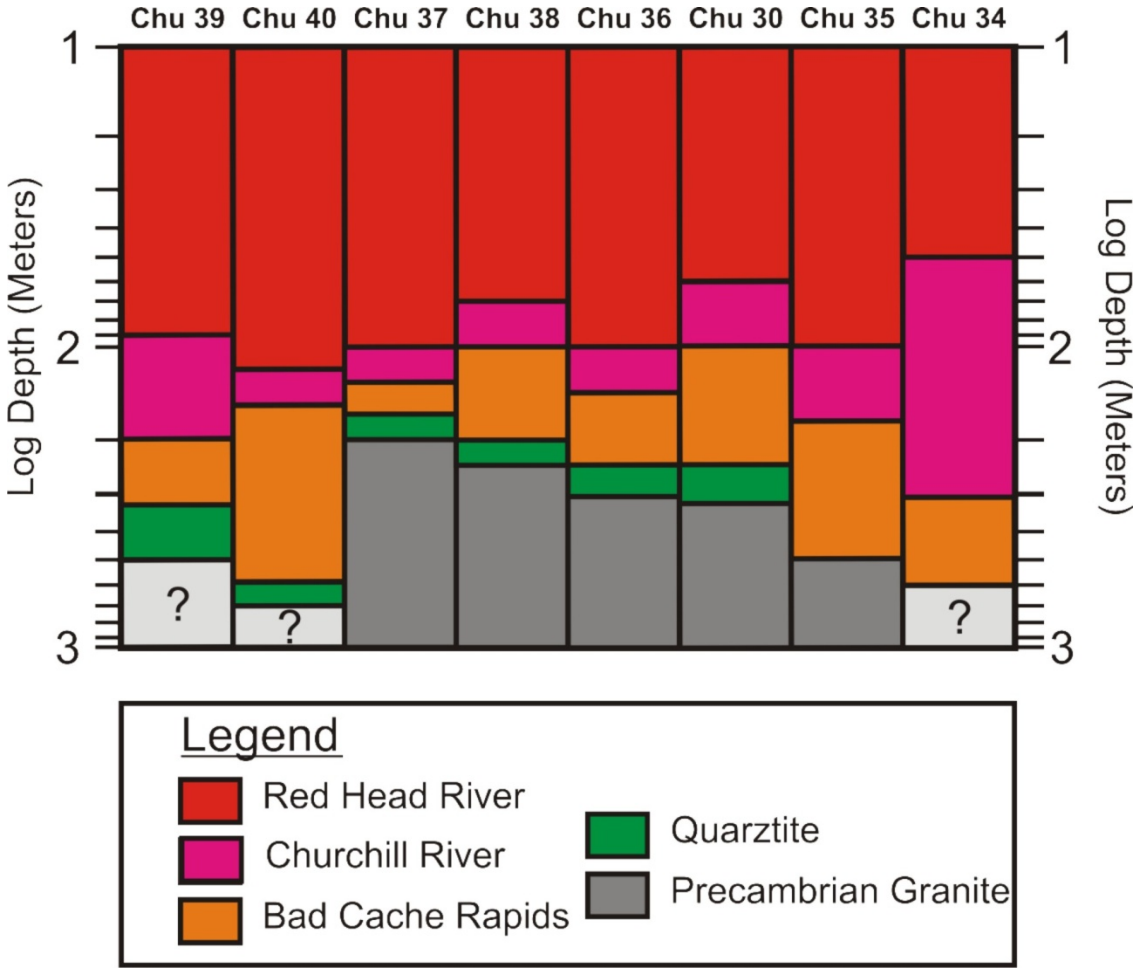

Figure 7: Schematic cross-section of geological strata for the eight sites of this study based on the inversion of the MT data and rock property data.

Conclusions

The MT data collected near Churchill, MB are affected by a variety of noise sources related to the electrical systems at the airport and power generation for the town. Exposure to these noise sources in such locales is unavoidable; however, careful selection of data and the general layered stratigraphy in the region enabled useful models of the subsurface to be achieved. The known stratigraphy enables the resulting 1-D models to be interpreted in terms of the actual rock formations in the region even though the resistivities derived from the core samples are non-unique.

The MT data validated by the rock property measurements resolve reasonably well the transition between the Churchill River and Bad Cache Rapids groups due to the significant difference in resistivity values between the dolostones of the Churchill River Group to the sandstones of the Bad Cache Rapids Group. Transitions at the Precambrian contact and between the Red Head River and Churchill River Formations are less well-resolved to to the overlaps in rock properties. Overall, the consistency of the models derived from the rock property data with the general stratigraphic framework for the region indicates MT is a useful tool for local or regional exploration of the Hudson Basin. The cross-section in the study area suggests the basin deepens abruptly west of Churchill between sites Chu 40 and Chu 37, perhaps due to faulting; although it is possible that noise in the data sensitive to the deeper elements of the stratigraphy may have impacted on the ability of MT to resolve this feature. It is unlikely noise in the data will be an issue when a site is located well away from man-made noise sources and therefore MT is a useful reconnaissance tool in this region and regions with similar straigraphy

Acknowledgements

The authors would like to acknowledge Jennifer Tigner and Devin Cowan who carried out the rock property measurements on the core resistivity samples in the GSC Paleomagnetism and Petrophysics Laboratory.

References

Chave, A. D., & Jones, A. G. (Eds.), 2012, Introduction to the magnetotelluric method. Cambridge University Press, 552p.

Constable, S. C., Parker, R. L., & Constable, C. G., 1987, Occam's Inversion: A practical algorithm for generating smooth models from electromagnetic sounding data. *Geophysics, 52*(3), 289-300.

Hamblin, A.P., 2008, Hydrocarbon potential of the Paleozoic succession of Hudson Bay/James Bay: Preliminary conceptual synthesis of background data. Geological Survey of Canada, Open File 5731, 12 p.

Heywood, W.W. and Sanford, B.V.,1976, Geology of Southampton, Coats and Mansel Islands, District of Keewatin, Northwest Territories. Geological Survey of Canada, Memoir 382, 35 p.

Kushnir, A., Andrews, G, Russell, J., Enkin, R., Kennedy, L., & Heap, M., 2012, Rock Physical-Property Measurements for the Nechako Basin Oil and Gas Region, Central British Columbia (Parts of NTS 093B, C, E, F, G, K, L). *Geoscience BC Summary of Activities 2011, Geoscience BC Report 2012-1,*, 125-150.

Lavoie, D., Pinet, N., Dietrich, J., Zhang, S., Hu, K., Asselin, E., Chen, Z., Bertrand, R., Galloway, J., Decker, V., Budkewitsch, P., Armstrong, D., Nicolas, M., Reyes, J., Kohn, B P., Duchesne, M J., Brake, V., Keating, P., Craven, J., Roberts, B., 2013, Geological framework, basin evolution, hydrocarbon system data and conceptual hydrocarbon plays for the Hudson Bay and Foxe basins, Canadian Arctic, Geological Survey of Canada, Open File 7363, 2013, 210 pages, doi:10.4095/293119

Lavoie, D., Zhang, S. and Pinet, N., 2011, Hydrothermal dolomites in Hudson Bay platform: preliminary field and geochemical data, Geological Survey of Canada, Open File 7002., 22 pages, doi:10.4095/289303

Nelson, S.J. 1963, Ordovician paleontology of the Hudson Bay Lowlands. Geological Society of America, Memoir 90, 152 p.

Nelson, S.J., 1964, Ordovician stratigraphy of northern Hudson Bay Lowlands, Manitoba. Geological Survey of Canada, Bulletin 108, 36 p. of Petroleum Geologists Bulletin, v. 65, n. 6, p. 1166–1175.

Nelson, S.J. and Johnson, R.D. 1966, Geology of Hudson Bay, Bulletin of Canadian Petroleum Geology. v. 14, n. 4, p. 520–578.

Norris, A.W. 1993. Hudson Platform – Geology. In: Sedimentary cover of the craton in Canada. D.F. Stott and J.D. Aitken (eds.). Geological Survey of Canada, Geology of Canada, n. 5, p. 653–700 (also Geological Society of America, The Geology of North America, v. D-1).

Roberts, B., & Craven, J., 2012, Results of a Magnetotelluric Survey in Churchill, Manitoba: GEM Energy, Hudson Bay. Geological Survey of Canada.

Sanford, B.V., Norris, A.W. and Bostock, H.H. 1968. Geology of the Hudson Bay Lowlands (Operation Winisk), Geological Survey of Canada, Paper 67-60, 118p

Zhang, S. and Barnes, C.R. 2007. Late Ordovician–Early Silurian conodont biostratigraphy and thermal maturity, Hudson Bay Basin. Bulletin of Canadian Petroleum Geology, v. 55, n. 3, p. 179–216.

Zhang, S., 2008, New insights into Ordovician oil shales in Hudson Bay Basin: their number, stratigraphic position, and petroleum potential, Bulletin of cabnadian Petroleuem Geology, v.56, NO. 4, P. 300–324.

Zhang, S. ,2010, Upper Ordovician Stratigraphy and Oil Shales on Southampton Island Field Trip Guidebook.

Appendix 1. AAV Models, comparison

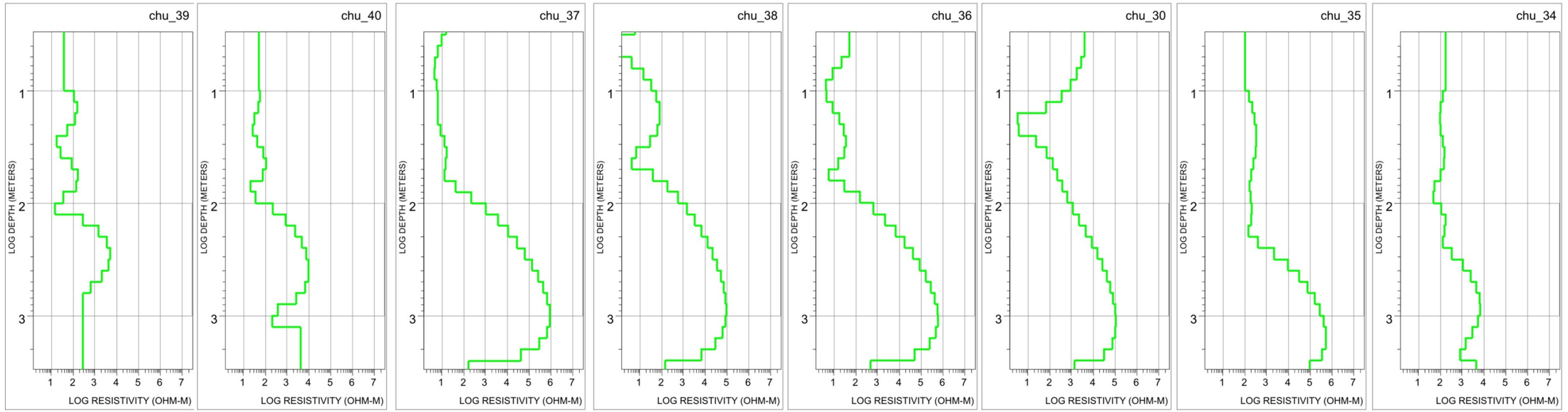

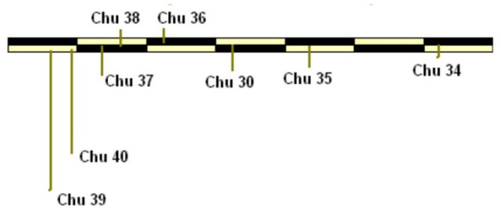

Figure 8: 1-D Inversion results from arithmetic averages of data. Pseudo-scale bar shows relative separation between sites along the dashed line in Figure 1.

Appendix 2. Averaged Data and Fit Curves from the 1-D Inversion

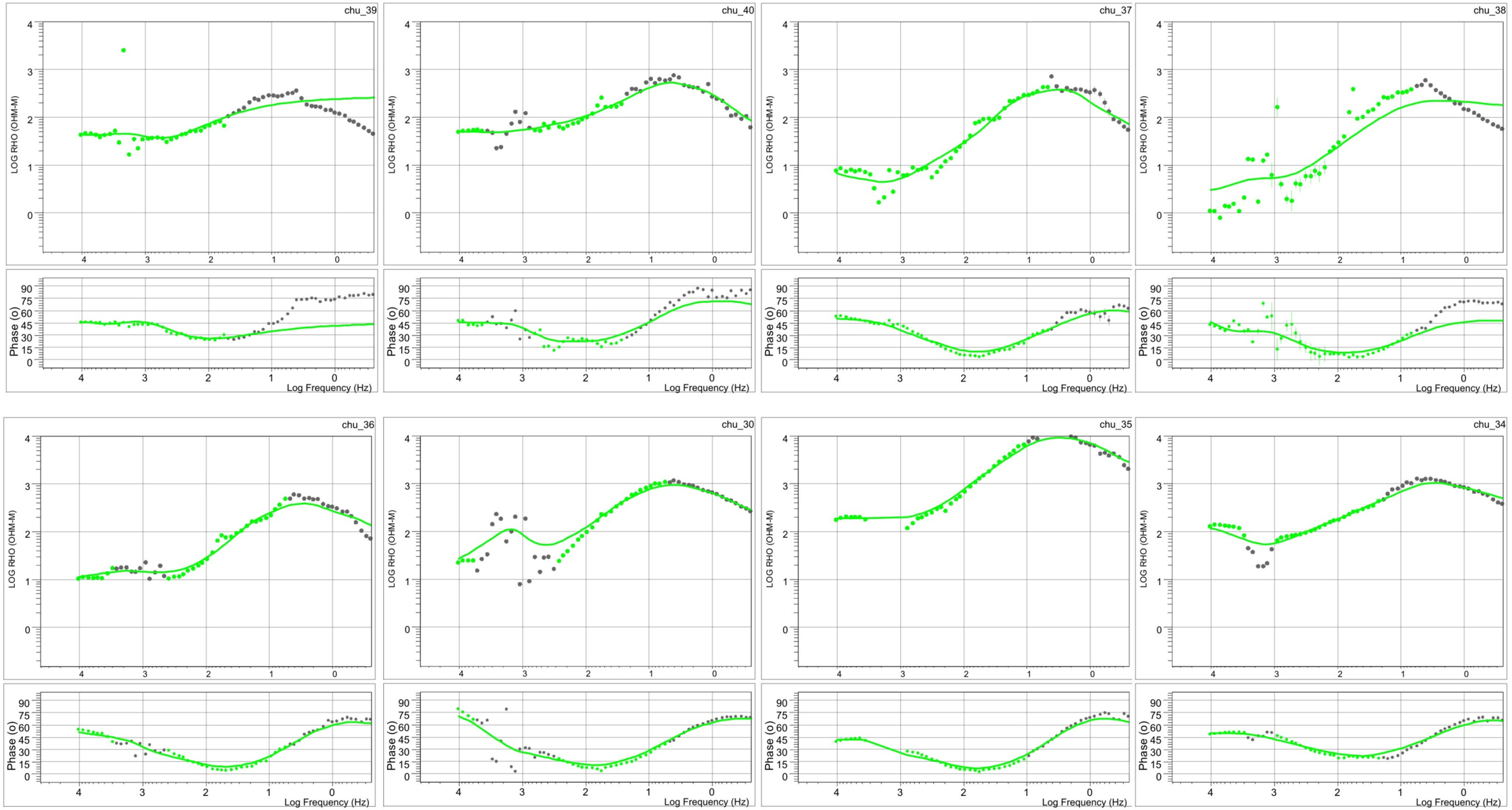

Figure 9: Averaged apparent resistivity and phase diagrams with the fit curved obtained from the inversion. Data in grey were not used in the inversion.

Appendix 3: Sample Rock Property Data

Sample #	Lab ID	Depth	Lithology Notes	Sat Bulk Density [g/cc]	Porosity (Connected) [%]	Magnetic Susceptibility [SI]	Resistivity [Ohm.m]	Chargeability [ms]
M-2-2001-1	MB-00001	102.7	Precambrian quarztite (fresh)	2.672	0.31	1.48E-04	4858	11.9
M-2-2001-2	MB-00002	101.54	Precambrian quarztite (fresh)	2.686	0.32	2.50E-04	5579	5.0
M-2-2001-3	MB-00003	99.75	Precambrian quarztite (weathered)	2.475	11.35	5.70E-05	1457	16.5
M-2-2001-4	MB-00004	97.25	Bad Cache Rapids Gp, Portage Chute Fm, Member 1; argillaceous sandstone	2.235	22.31	4.62E-05	430	1.4
M-2-2001-5	MB-00005	95.10	Bad Cache Rapids Gp, Portage Chute Fm, Member 1; argillaceous sandstone	2.213	25.89	3.17E-05	1681	1.5
M-2-2001-6	MB-00006	88.75	Bad Cache Rapids Gp, Portage Chute Fm, Member 1; coarse sandstone	2.394	15.84	2.03E-05	42	0.7
M-2-2001-7	MB-00007	85.90	Bad Cache Rapids Gp, Portage Chute Fm, Member 1; argillaceous sandstone	2.207	24.59	7.23E-06	4822	6.2
M-2-2001-8	MB-00008	83.65	Bad Cache Rapids Gp, Portage Chute Fm, Member 1; quartzose sandstone	2.197	24.49	-3.59E-06	7431	4.2
-2-2001-9	MB-00009	81.20	Bad Cache Rapids Gp, Portage Chute Fm, Member 1; quartzose sandstone	2.208	7.68	3.05E-06	9821	0.8
M-2-2001-10	MB-00010	76.80	Bad Cache Rapids Gp or Churchill River Gp(?); dolomitic wackestone	2.572	8.92	4.53E-05	330	8.0
M-2-2001-11	MB-00011	57.40	Bad Cache Rapids Gp or Churchill River Gp(?); sandy, dolomitic limestone	2.553	10.17	1.56E-05	73	0.1
M-2-2001-12	MB-00012	54.00	Bad Cache Rapids Gp or Churchill River Gp(?); dolomitic wackestone	2.528	11.96	1.03E-05	91	0.7
M-2-2001-13	MB-00013	47.90	Bad Cache Rapids Gp or Churchill River Gp(?); dolomitic limestone	2.534	12.34	5.30E-06	65	0.1
M-2-2001-14	MB-00014	41.25	Bad Cache Rapids Gp or Churchill River Gp(?); dolomitic wackestone	2.511	12.04	9.31E-06	79	1.3
M-2-2001-15	MB-00015	31.20	Red Head Rapids Fm; argillaceous, dolomitic mudstone	2.736	3.29	5.17E-05	377	3.2
M-2-2001-16	MB-00016	30.90	Red Head Rapids Fm; argillaceous, dolomitic wackestone	2.652	5.29	3.54E-05	195	10.7
M-2-2001-17	MB-00017	26.95	Red Head Rapids Fm; argillaceous, dolomitic mudstone	2.760	1.36	3.01E-05	2478	1.1
M-2-2001-18	MB-00018	24.00	Red Head Rapids Fm; dolomitic wackestone	2.683	6.26	4.41E-05	267	4.5
M-2-2001-19	MB-00019	19.70	Red Head Rapids Fm; porous dolomitic wackestone	2.561	13.53	4.70E-05	106	0.9
M-2-2001-20	MB-00020	13.25	Red Head Rapids Fm; argillaceous, dolomitic mudstone	2.674	7.39	4.27E-05	148	4.3
M-2-2001-21	MB-00021	12.85	Red Head Rapids Fm; dolomitic wackestone	2.502	17.15	2.21E-05	31	0.4
M-2-2001-22	MB-00022	6.75	Red Head Rapids Fm; dolomitic mudstone	2.406	22.9	3.69E-05	28	0.1
M-2-2001-23	MB-00023	3.20	Red Head Rapids Fm; mottled, porous, dolomitic mudstone	2.677	7.69	2.21E-05	771	0.8
M-2-2001-24	MB-00024	2.50	Red Head Rapids Fm; argillaceous, dolomitic mudstone	2.732	2.85	7.69E-06	7557	6.1
M-2-2001-25	MB-00025	0.20	Severn River Fm; dolomitic mudstone	2.637	6.39	2.47E-05	239	1.1
52-10-2277-A01	MB-00027	outcrop	Precambrian granite	2.671	0.24	2.04E-04	7343	4.6

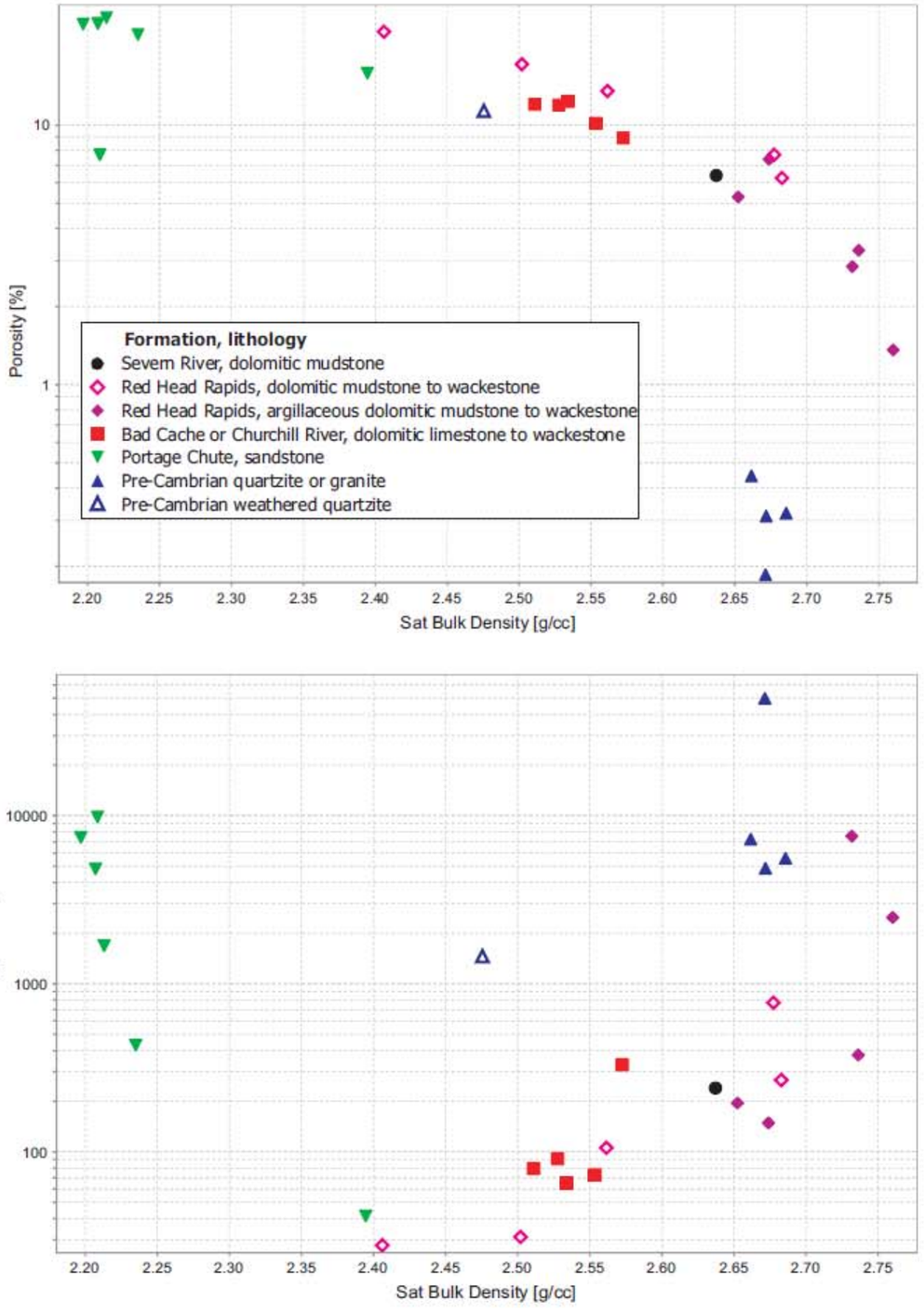

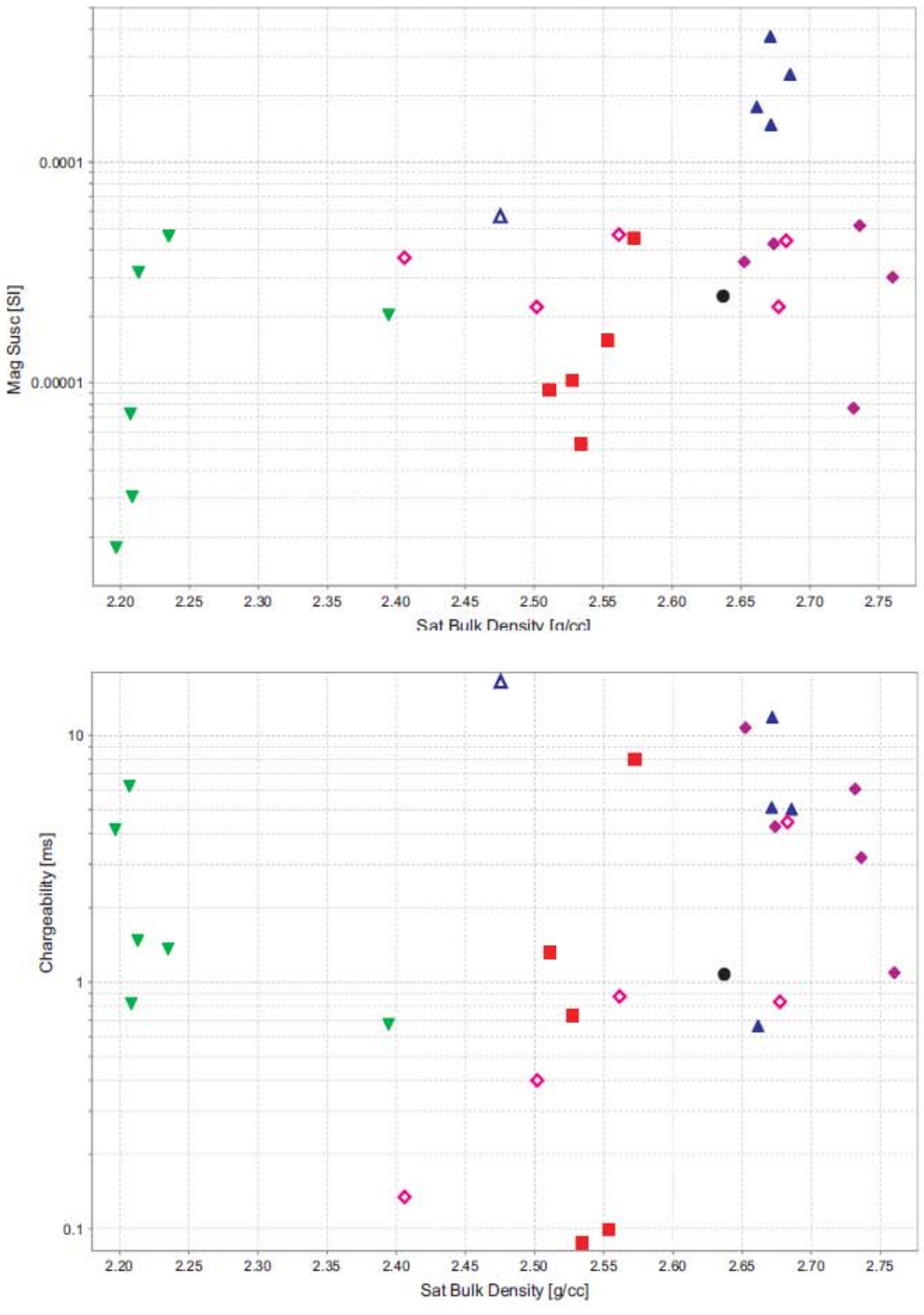

Figure 10: Petrophysical Data Plots.